

## A Study of Factors Influencing on Dissolution Behavior of Copper in Orthophosphoric Acid Using Rotating Cylinder Electrode (RCE) and Rotating Disc Electrode (RDE)

A.A.Taha\* H.H. Abdel Rahman,,A.M.Ahmed, F.M.Abouzeid

Chemistry Department, Faculty of Science, Alexandria University, Alexandria, Egypt

\*E-mail: [asia\\_taha@yahoo.com](mailto:asia_taha@yahoo.com)

Received: 30 April 2013 / Accepted: 28 May 2013 / Published: 1 July 2013

---

The rotating cylinder electrode (RCE) and rotating disc electrode (RDE) are used for investigation of dissolution behavior of copper in presence of surfactant (Triton x-100, SDS and CPC). The dissolution of copper was studied in 8M H<sub>3</sub>PO<sub>4</sub> as a function of surfactant concentration ( $5 \times 10^{-7}$  -  $1 \times 10^{-2}$  M) at 25°C. Measurements were conducted based on potentiodynamic polarization method. The inhibition behavior of low cost surfactants compounds was inspected. The inhibition efficiency of these surfactants was depending on their concentration and their chemical structure. The rotation speed of RCE and RDE effect was explored. The adsorption of surfactants on copper surface was found to be not obeying Langmuir and followed Kinetic-thermodynamic adsorption isotherm. Activation energy, the pre-exponential factor and adsorption free energy  $\Delta G^{\circ}_{ads}$ , are calculated and discussed. Scanning electron microscope (SEM) was used to characterize the copper surface. Different reaction conditions and the physical properties of solutions are studied to obtain dimensionless correlation among all these parameters. Experimental result showed that the inhibition efficiency of SAS improved in presence of alcohols. The synergism parameters are found to be greater than unity indicating that co-operative adsorption of alcohols and SAS.

---

**Keywords:** Copper; rotating cylinder electrode (RCE); rotating disc electrode (RDE); surfactants; scanning electron microscope (SEM).

### 1. INTRODUCTION

In spite of much advancement in the field of corrosion science and technology, the phenomenon of corrosion (mainly of Fe, Al, Cu, Zn, Mg and their alloys) remains a major concern to industries around the world. Copper and its alloys have a long history of use in marine applications and continue to be widely used for many purposes despite the emergence in recent years of other materials

that have technical or economic attraction. These related to their corrosion resistance, mechanical workability excellent electrical, thermal conductive and resistance to microfouling. Copper alloys have gained increasing importance for applications sea water environments such as heat exchangers of power plants. Scale and corrosion products cause a decrease in the heating efficiency of the equipment, which is why periodic descaling and cleaning in acid-pickling solutions are necessary. In order to reduce the corrosion of the copper alloys during such Surface treatments, a corrosion inhibitor is typically added [1, 2].

It is well known that corrosion never stops but its scope and severity can be lessened. The addition of surfactants into aggressive media such as acid solutions is one of the methods for achieving this goal. Surfactants are organic molecules that have a chemical structure combining both a polar (amphiphobic) and a nonpolar (amphiphilic) group into a single molecule. When dissolved in a solvent at low concentration, they have the ability to adsorb (or locate) at interfaces, thereby alter significantly physical properties of the interfaces. Micellization is observed in surfactant solutions when concentration exceeds the critical micelle concentration (CMC), whereas the physicochemical properties of the aqueous solution change abruptly [3].

Surfactants are compounds that can be found in a multitude of domains, from industrial settings to research laboratories and are the part of our daily lives. Due to their unique structure they can drastically modify the interfacial properties. This effect is important for industrial processes such as flotation, the cosmetic and food industries, drugs delivery, emulsification, chemical mechanical polishing, as also for corrosion inhibition [4,5].

The majority of the studies on the dissolution of metals have been carried out under the static conditions; therefore, the influence of flow on the dissolution process is an important issue to be considerable in the design and operation of industrial equipment. The most common type of flow conditions found in industrial processes is turbulent; however, few dissolution studies in controlled turbulent flow conditions are available. With the increasing necessity to describe the dissolution of metals in turbulent flow conditions, some laboratory hydrodynamic systems such as rotating cylinder electrode (RCE) are used [6]. The use of rotating cylinder and disc electrode in dissolution process , fluid flow cause an increase in the rate of transport of chemical species to/from the metal surface , resulting in an increase of dissolution rate [7].

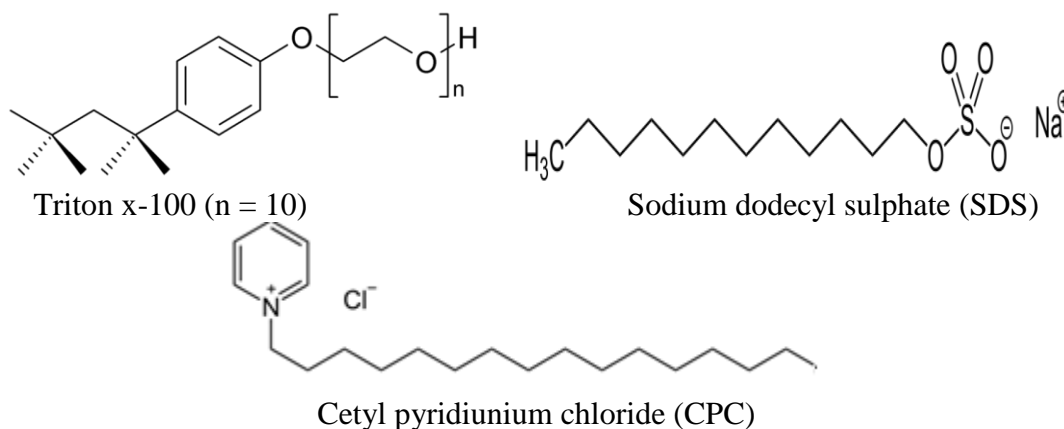
Phosphoric acid ( $H_3PO_4$ ) is widely used in the production of fertilizers and surface treatment of steel such as chemical and electrolytic polishing or etching, removal of oxide film, phosphating, passivating, and surface cleaning [8]. The corrosion of copper in phosphoric acid was studied previously in the presence of alcohols [9], amines [10], aldehydes [11], and amino acids [12]. Hence, the aim of this work is to examine the dissolution behavior of rotating copper anode in  $H_3PO_4$  in presence of surfactants (SAS) namely Triton x-100, anionic surfactant namely sodium dodecyl sulphate (SDS) and cationic surfactant namely cetyl pyridinium chloride (CPC). The adsorption of the surfactants on the metal surface can markedly change the dissolution –resisting property of the metal, so the study of the relationship between the adsorption and dissolution inhibition is of great importance.

## 2. MATERIAL AND METHOD

### 2.1. Potentiodynamic measurements

The apparatus used in the present work consists of the cell and the electrical circuit. The cell consisted of 15 cm diameter cylindrical plexiglass container of 30 cm height. The anode was a rotating copper rod connected to the shaft of a variable speed motor through a plastic sleeve and copper cylindrical cathode lining the inner wall of the container. The anode diameter is 2 cm was used, the working area of the cylindrical anode is  $12.56 \text{ cm}^2$  while the anodic disc is  $3.14 \text{ cm}^2$ . Rotation speed of rotating anode which ranged from 0 to 750 rpm was controlled with a variac and was measured by an optical tachometer. The electrical circuit consisted of a 6V D.C. power supply, a multi range ammeter connected in a series with cell. A voltmeter was connected in parallel with the cell to measure its potential. 8 M phosphoric acid was prepared from analar grade  $\text{H}_3\text{PO}_4$  (85%). Ten concentrations of surfactant solutions (Triton x-100, Sodium dodecyl sulphate and Cetyl pyridinium chloride) with 8 M  $\text{H}_3\text{PO}_4$  are used ranging from  $5 \times 10^{-7}$  to  $1 \times 10^{-2}$  M. In view of the large cathode area compared to the anode area, the cathode was taken as a reference electrode against which the anode potential was measured. The limiting current was determined from the current –potential curves (polarization curves) which were plotted by increasing the applied current stepwise and measuring the corresponding steady-state potential. Two minutes were allowed for reaching the steady state potential. Before each run, the anode was insulated with polystyrene lacquer and the active surface was polished with fine emery paper, degreased with trichloroethylene, washed with alcohol and finally rinsed in distilled water with a measured conductance  $5.5 \times 10^{-6} \text{ S/m}$ . The temperature was regulated by placing the cell in thermostatic water bath at different temperatures (25, 30, 35 and  $40^\circ \text{C}$ )  $\pm 0.5^\circ \text{C}$ . The copper used in this study of 99.98 weight % purity (0.001Cd, 0.001 Ag, 0.003Pb and 0.005Sn)

The structure of SAS is given below:



### 2.2. Surface tension measurements

The surface tension was measured at  $25^\circ \text{C}$  using Du Nouy tensiometer (Kruss type 8451) for various concentrations of the surfactants additives. The temperature was kept constant by circulating the thermostatted water through a jacketed vessel containing the solution ( $\pm 0.5^\circ \text{C}$ ). The critical micelle concentration (CMC) was determined from the surface tension measurements at different SAS

concentrations and checked by performing at least three separate experiments. The obtained (CMC) values of the studied SAS are  $5 \times 10^{-5}$ ,  $5 \times 10^{-4}$  and  $1 \times 10^{-3}$  mol/l for Triton x-100, SDS and CPC respectively [13].

### 2.3. Density and viscosity measurements

The density was measured by using DA-300 Kyoto electronic instrument. The viscosity was measured by using Koehler viscosity bath (model K23400) (Table 1). The accuracy of the instrument is 2%.

**Table 1.** Physical properties of  $H_3PO_4$  solution in the absence and presence of SAS at 25° C

SAS Conc. mol l <sup>-1</sup>	Triton x-100			SDS			CPC		
	$\rho$ (g.cm <sup>-3</sup> )	$\mu$ (g.cm <sup>-1</sup> .sec <sup>-1</sup> )	$10^6 D$ (cm <sup>2</sup> .sec <sup>-1</sup> )	$\rho$ (g.cm <sup>-3</sup> )	$\mu$ (g.cm <sup>-1</sup> .sec <sup>-1</sup> )	$10^6 D$ (cm <sup>2</sup> .sec <sup>-1</sup> )	$\rho$ (g.cm <sup>-3</sup> )	$\mu$ (g.cm <sup>-1</sup> .sec <sup>-1</sup> )	$10^6 D$ (cm <sup>2</sup> .sec <sup>-1</sup> )
			RCE RDE			RCE RDE			RCE RDE
0.0	1.2312	0.04200	1.92 3.55	1.2312	0.04200	1.92 3.55	1.2312	0.04200	1.92 3.55
5.0E-07	1.2516	0.05044	1.00 1.75	1.2330	0.04291	1.53 3.04	1.2817	0.05070	3.51 2.65
1.0E-06	1.2602	0.05121	0.77 1.55	1.2508	0.04388	1.02 2.89	1.2857	0.05184	2.42 2.29
5.0E-06	1.2702	0.05230	0.59 1.30	1.2695	0.04606	0.87 2.52	1.2932	0.05273	1.80 1.96
1.0E-05	1.2763	0.05305	0.45 1.11	1.3012	0.04647	0.70 2.03	1.3057	0.05373	1.20 1.57
5.0E-05	1.2831	0.05054	0.57 1.31	1.3043	0.05230	0.56 1.83	1.3077	0.05436	0.91 1.33
1.0E-04	1.2947	0.05106	0.46 1.24	1.3116	0.05267	0.47 1.56	1.3085	0.05519	0.73 1.10
5.0E-04	1.2989	0.05300	0.39 1.13	1.3146	0.05312	0.41 1.34	1.3108	0.05615	0.66 0.88
1.0E-03	1.3053	0.05423	0.36 1.06	1.3250	0.05759	0.37 1.18	1.3148	0.05101	0.62 1.01
5.0E-03	1.3111	0.05506	0.33 0.96	1.3292	0.06141	0.33 1.05	1.3157	0.05058	0.66 1.13
1.0E-02	1.3172	0.05667	0.32 0.72	1.3386	0.06522	0.30 0.91	1.3173	0.04660	0.67 1.23

### 2.4. Diffusion coefficients measurements

The diffusion coefficient of blank solution and of solutions in the presence of different concentrations of SAS (Table 1) used in this study were calculated by measuring the limiting current of the anodic dissolution of a copper rotating disc in  $H_3PO_4$  and applying the Levich equation [9].

$$i_L = 0.62 n F D_{\text{eff}}^{2/3} \nu^{-1/6} (C_{\text{sat,Cu}} - C_{\text{b,Cu}}) \omega^{1/2} \quad (1)$$

While Eisenberg equation applied to calculate diffusion coefficient for copper dissolution using rotating cylinder electrode [14].

$$i_L = 0.0791 n F C \omega^{0.7} d^{-0.3} \nu^{-0.344} D^{0.644} \quad (2)$$

where  $i_L$  is the limiting current density  $i_L = I_L/A$  (A.cm<sup>-2</sup>) and A is the cross-sectional area of Cu disc or cylinder, n is the number of electrons involved in the reaction, F is Faraday constant, D is the diffusion coefficient of dissolving species,  $\nu$  is the kinematic viscosity,  $\omega$  is the electrode rotation rate ( $\omega = 2\pi \text{ rpm} / 60$ ),  $C_{\text{sat,Cu}}$  is the saturation concentration of dissolved species and  $C_{\text{b,Cu}}$  is the bulk concentration which is zero. The saturation solubility of copper phosphate in different  $H_3PO_4$  concentrations was determined by using Perkin Elmer 2380 atomic absorption spectrophotometer.

### 2.5. Scanning electron microscope (SEM)

The scanning electron microscope images were taken using (JEOL, JSM-5300, scanning microscope, OXFORD instrument).

## 3. RESULTS AND DISCUSSIONS

### 3.1. Polarization studies

Fig.1 shows polarization curve for copper RDE in 8M H<sub>3</sub>PO<sub>4</sub> in the absence and presence of various concentration of Triton x-100 as an example. It is clear that the presence of SAS causes a markedly decrease in the dissolution rate. This may be ascribed to adsorption of SAS over the copper surface [15, 16]. The values of limiting current ( $I_L$ ) and inhibition efficiency percentage (IE %) as function of SAS concentration for RDE and RCE are represented in Table2.

The inhibition efficiency percentage (IE %) was calculated using the following equation :

$$IE\% = \frac{I_{L(blank)} - I_{L(SAS)}}{I_{L(blank)}} \times 100 \quad (3)$$

Where  $I_{L(blank)}$  and  $I_{L(SAS)}$  are the limiting current of dissolution process without and with SAS respectively .

The inhibition behavior differ from surfactant to another , in case of Triton x-100, limiting current of dissolution process decrease as concentration increase up to CMC value, at CMC value ( $5 \times 10^{-5}$ ), limiting current increases while when concentration exceed CMC, limiting current decrease as Triton x-100 concentration increase (Table 2). The inhibition behavior of Triton x-100 was explained on the basis of poly centric adsorption, which may take place as a result of the existence of many oxygen atoms in the molecules. The interaction occurs between unshared electron pair and metal surface in addition to protective layer formed by alkyl chain length which decreases the anodic dissolution of copper metal. The high performance of Triton x-100 was attributed to presence of many adsorption centers, large molecular size and the planarity of the compound [17]. The molecules can lay flat to the surface and can also be oriented perpendicularly , in the first orientation, the hydrocarbon chain also interact with metal surface so limiting current decrease and inhibition percentage increase while at second orientation (expected when micelle formed, CMC) the molecules of Triton x-100 form a porous monolayer with strong lateral interaction between SAS molecules so IE % decrease, at higher concentration of Triton x-100 , the surface is saturated and protective bilayer is formed so IE% increase [18].

In case of SDS, the limiting current decrease and IE % increase as SDS concentration increase although the concentration exceed the critical micelle concentration. The inhibition action of SDS due to electrostatic interaction between negatively charged anionic surfactant SDS and positively charged copper anode. A great change in the dissolution process is observed jointly with a more significant decrease of limiting current at concentration higher than  $5 \times 10^{-4}$ . It might be explained by micellization above critical micelle concentration where maximum efficiency is obtained , at or above this CMC ,

the SDS molecules in solution forms a surfactant bi-layer (ad micelles ) on copper surface so IE% increase [18-20].

While the inhibition behavior of the third studied surfactant CPC, it was found that delocalization of  $\pi$  orbital in the pyridine may increase the positive charge on nitrogen atom of the ring which difficult to approach the positively charged copper surface due to repulsion, the presence of  $Cl^-$  make the surface charge of copper metal is changed to negative by the specific adsorption of the anion with the cation. Further, adsorption of some ions has been suggested to involve not only electrostatic interaction but also partial charge transfer leading to covalent bond formation. The acceleration in dissolution of copper observed after  $5 \times 10^{-4}$  mol/l can be attributed to when CPC micelle formed at  $1 \times 10^{-3}$  mol/l which carry concentrated positively charged heads with concentrated negatively charged chloride counter ions, the higher concentration of aggressive chloride ions which lead to copper dissolution promotion [21].

It is obvious from (Fig.2 & Table 2) that the inhibitive behavior of SAS is a function of concentration. If the SAS are compared according to maximum inhibition efficiency, they are ranked as follow

Triton x-100 > SDS > CPC (before CMC)

SDS > Triton x-100 > CPC (after CMC)

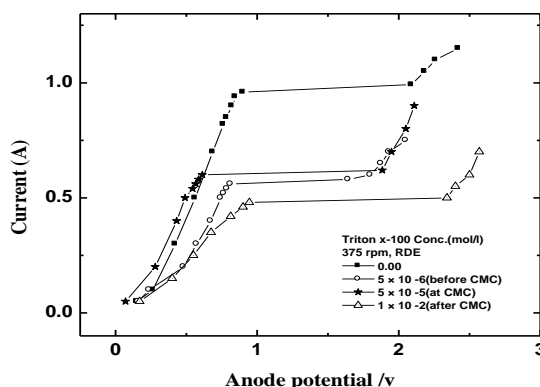


**Figure 1.** Polarization curve of copper RDE dissolution in 8M  $H_3PO_4$  in the absence and presence of different concentrations of Triton x-100 at 25°C.

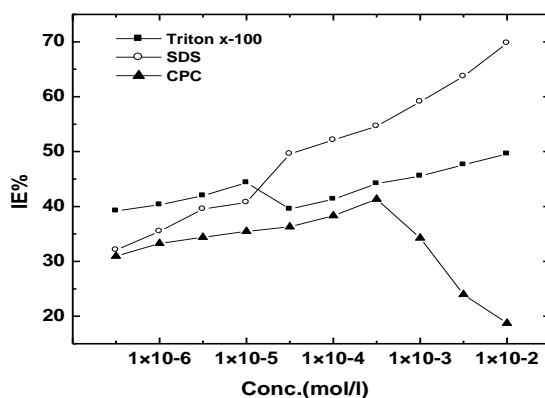


**Figure 2.** Inhibition efficiency percentage, (IE %) as a function of SAS for copper RDE at 25°C and 375 rpm.

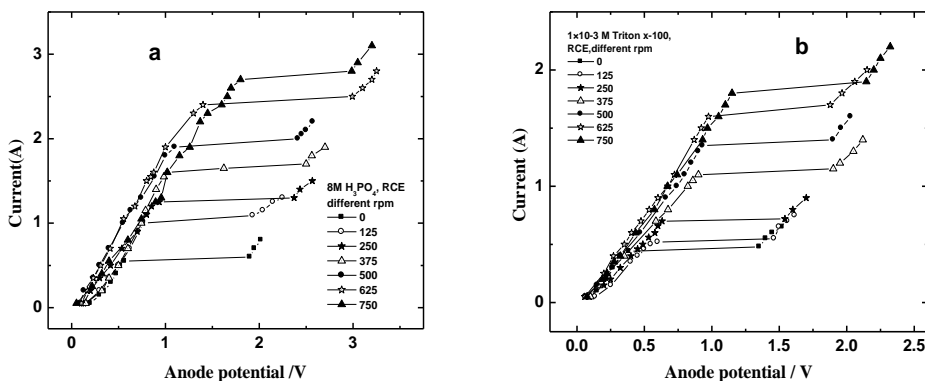
3.2. Effect of stirring

Fig. 3 shows typical polarization curve with a well defined limiting current plateau obtained for the anodic rotating cylinder and disc copper electrode at different rotations speeds. The curve shows three zones: the mixed control region where the primary reaction is controlled by both mass transport and electron transfer; the plateau region where the primary reaction is under complete mass transport control, and the final section where a secondary reaction (typically oxygen evolution) occurs at the same time as the primary reaction. The limiting current arises due to convective- diffusion of the reactant toward the electrode, and the presence of the plateau indicate that the transport of ions to the working electrode achieved a maximum rate and is the determining step [22]

It is clear that the measured limiting current is affected by rotation rate of the electrode, as the rotation rate of the electrode increases the measured value of limiting current also increase. According to Grimm and Landolt [23] under these conditions , dissolution rate is mass transport controlled and involves diffusion and migration of metal ions through a stagnant (Nernst ) diffusion layer so the thickness of diffusion layer depend on rotation rate. It is evident from Fig. 3a-d that increases in rotation rate, the height of the plateau (magnitude of limiting current) increases. Based on the above statement, the increase in the rotation rate decrease the thickness of the Nernst diffusion layer, causing shorter path length for the diffusion of ions and hence a higher magnitude of limiting current and limiting current density.

Fig. 4 compares the different measured and calculated current densities as a function of  $\omega$  to a power of 0.7 in 8 M  $H_3PO_4$  in presence of  $10^{-2}$  M of SAS at  $25^\circ C$  (as an example). The analysis of Fig.4 confirms that, as the rotation rate of the electrode increases the measured limiting current also increases. It is also possible suggest that the measured limiting current can be associated to the diffusion of  $Cu^{2+}$  ions [6]

Based on Levich behavior at the rotating disk electrode, Fig .5a shows a that the values of  $i_L$  is proportional to  $\omega^{0.5}$  at all velocity and in absence and presence of  $10^{-2}$  M SAS indicating that dissolution of copper electrode in absence and presence of SAS is under mass transfer conditions. A plot of the reciprocal of the plateau current density as a function of the reciprocal of the square root of disk rotation speed should form a straight line passing through the origin in the absence and presence of SAS (Fig.5b). This behavior confirms the dissolution of copper at the current plateau was mass transport controlled [24-28].



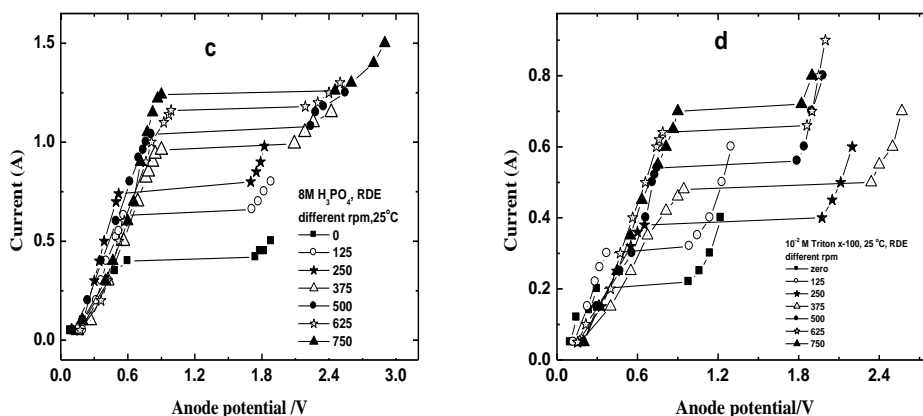


**Figure 3.** Anodic polarization curve for rotating anode copper electrode at different rotations speeds in a) 8 M H<sub>3</sub>PO<sub>4</sub> acid (RCE). b) 8 M H<sub>3</sub>PO<sub>4</sub> + 10<sup>-3</sup> M Triton x-100 (RCE), c) 8 M H<sub>3</sub>PO<sub>4</sub> (RDE) and d) 8 M H<sub>3</sub>PO<sub>4</sub> + 10<sup>-3</sup> M Triton x-100 (RDE) at 25°C.

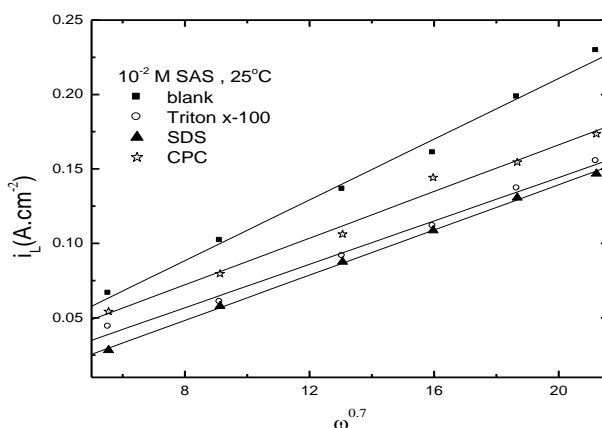


**Figure 4.** Variation of current density,  $i_L$  with angular velocity,  $\omega$  to a power of 0.7 in 8 M H<sub>3</sub>PO<sub>4</sub> in absence and presence of 10<sup>-2</sup> M of SAS at 25°C.

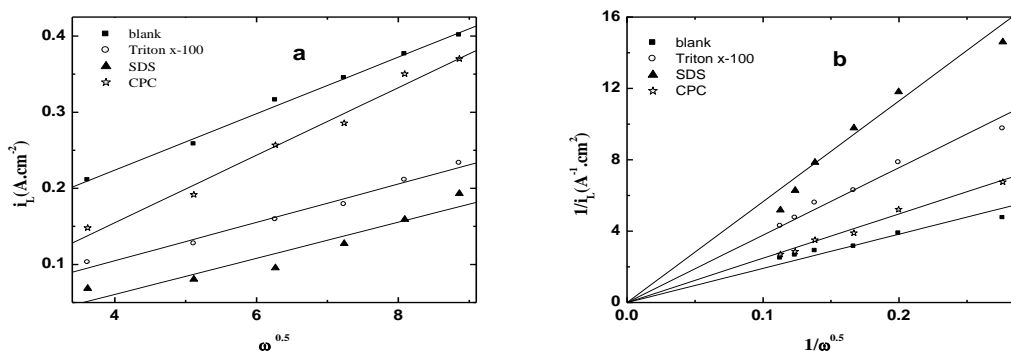


**Figure 5.** (a) Levich plot, current density  $i_L$  as a function of  $\omega^{0.5}$ , in 8 M H<sub>3</sub>PO<sub>4</sub> in the absence and presence of 10<sup>-2</sup> M of SAS at 25°C. (b) Koutecky –Levich plot,  $i_L^{-1}$  as a function of  $\omega^{-0.5}$  in 8 M H<sub>3</sub>PO<sub>4</sub> in the absence and presence of 10<sup>-2</sup> M of SAS at 25°C.

3.3. Temperature effect and activated parameters of dissolution process

Temperature is an important parameter in studies of metal dissolution. To verify the effect of temperature on the dissolution process for copper RDE and RCE in 8M H<sub>3</sub>PO<sub>4</sub> in the absence and presence of different concentrations of SAS, the experiment were undertaken in this study in the temperature range of 25-40°C .Results obtained indicate that dissolution rate increases with increase in temperature in the absence and presence of SAS (Fig.6) due to enhanced effect of temperature on the dissolution process [29, 30].

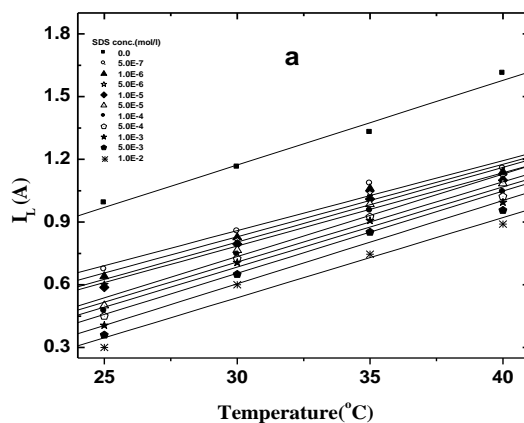


**Figure 6.** Variation of: limiting current ( $I_L$ ) with temperature at different concentrations of SDS for copper RDE at 375rpm.

The comparison of values of activation energy and the pre-exponential factor of the dissolution process in the absence and presence of SAS is commonly used to evaluate the adsorptive behavior of SAS molecules on copper surface [31]. The dependence of the dissolution rate on temperature was expressed by the Arrhenius equation:

$$\ln I_L = \ln A - E_a/RT \tag{4}$$

Where A is the pre-exponential factor,  $E_a$  is the activation energy of copper dissolution reaction, R is gas constant and T is the temperature.

Fig. 7 shows the Arrhenius plots for the dissolution of copper with and without 10<sup>-3</sup> M SAS for RCE as an example, the plots obtained are straight lines and each regression coefficient was close to 1, indicating that the linear relation between  $\ln I_L$  and 1/T are good. The slope of each straight line gave its activation energy, and intercept gave the pre-exponential factor. The results were summarized in Table 2. The calculated activation energies are bigger than those of blank, suggesting the higher energy barrier for the dissolution of the inhibited specimens.

The higher  $E_a$  values in presence of SAS in compared to 8 M H<sub>3</sub>PO<sub>4</sub> free solution can be attributed to the decrease in surface area available for dissolution, because dissolution primary occurs at surface sites free of adsorbed SAS molecules [32] and this behavior indicates the physical adsorption behavior of the three studied surfactants [33].According to equation (4), it can be seen that, the lower pre-exponential factor A and higher activation energy  $E_a$  lead to lower in dissolution rate,  $I_L$ , for the present study, the values of A in the presence of SAS are higher than that in the absence of

SAS. Therefore, the decrease in copper dissolution rate is mostly decided by the activation energy [15].

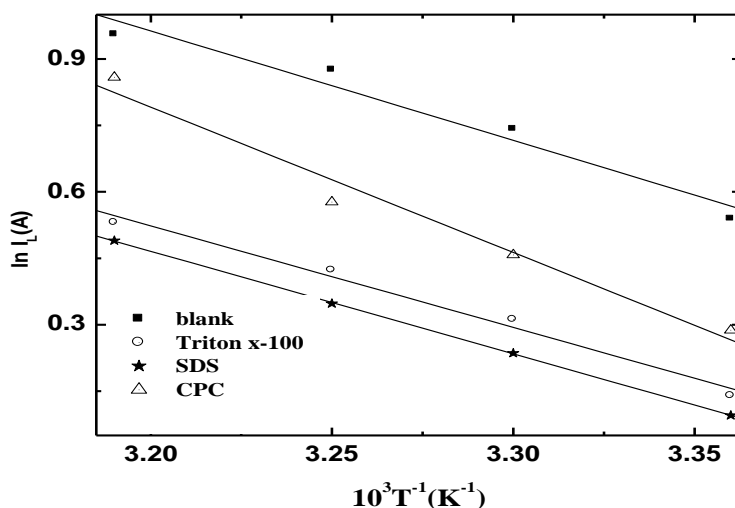


**Figure 7.** Arrhenius plot of the dissolution process recorded for RCE copper at 375 rpm in 8M H<sub>3</sub>PO<sub>4</sub> solution containing 10<sup>-3</sup> M of SAS.

The activated parameters for the dissolution process were calculated the following equations:

$$\Delta H^\# = Ea - RT \tag{5}$$

$$I_L = RT/Nh \exp(\Delta S^\#/R) \exp(-\Delta H^\#/RT) \tag{6}$$

$$\Delta G^\# = \Delta H^\# - T\Delta S^\# \tag{7}$$

Where h is the plank' s constant, N is the Avogadro's number,  $\Delta H^\#$  is the enthalpy of activation,  $\Delta S^\#$  is the entropy of activation and  $\Delta G^\#$  is free energy of activation. The data of activation parameters of the dissolution process are represented in Table 2 which indicates that the addition of surfactants to the dissolution medium leads to an increase in the  $\Delta H^\#$  values; so these molecules increase the height of energy barrier for the dissolution process.

In addition, the values of entropy of activation  $\Delta S^\#$  are large and negative. This implies that the activated complex in the rate determining step represent association rather than dissociation meaning that the decrease in the disordering which takes place on going from reactants to the activated complex [34]. In other words, surfactant is randomly presented in the solution, but when it is migrated to the metal surface, it will be ordered on the metal surface. Hence, there will be a decrease in the disorder, so that the  $\Delta S^\#$  is negative value. The weak dependence of  $\Delta G^\#$  on the composition of SAS can be attributed largely to the general linear compensation between  $\Delta H^\#$  and  $\Delta S^\#$  for the given temperature [35].

**Table 2.** Values of limiting current  $I_L(A)$  , IE % at 25°C and activated parameters using RDE and RCE in 8M  $H_3PO_4$  in absence and presence of SAS at 375 rpm.

Conc. (mol/l)	SAS	RDE						RCE							
		$I_L(A)$	IE%	Ea (kJ/mol <sup>-1</sup> )	$A \cdot 10^{-3}$	$\Delta H^\ddagger$ (kJ/mol)	$-\Delta S^\ddagger$ (J/mol.K)	$\Delta G^\ddagger$ (kJ/mol)	$I_L(A)$	IE%	Ea (kJ/mol <sup>-1</sup> )	$A \cdot 10^{-3}$	$\Delta H^\ddagger$ (kJ/mol)	$-\Delta S^\ddagger$ (J/mol.K)	$\Delta G^\ddagger$ (kJ/mol)
0.0	Triton x-100	0.992		24.67	20.33	22.19	170.60	73.05	2.6	21.54	10.40	<b>19.06</b>	176.24	71.61	
5.0E-07		0.603	39.21	33.25	416.64	30.77	145.48	74.46	2.080	20.00	25.50	33.52	23.03	166.44	72.65
1.0E-06		0.592	40.32	33.08	384.61	30.61	146.20	74.20	1.800	30.77	19.70	3.26	17.22	185.87	72.64
5.0E-06		0.576	41.94	33.75	488.94	31.28	144.20	74.27	1.780	31.54	23.30	13.06	20.82	174.34	72.80
1.0E-05		0.552	44.35	34.70	680.10	32.22	141.40	74.38	1.722	33.77	24.80	22.70	22.30	169.76	72.94
5.0E-05		0.600	39.52	36.23	1369.22	33.75	135.62	74.19	1.822	29.92	20.87	5.54	18.39	181.43	72.48
1.0E-04		0.582	41.33	34.89	766.81	32.41	140.45	74.29	1.772	31.85	20.00	3.86	17.54	184.41	72.53
5.0E-04		0.554	44.15	36.91	1639.66	34.43	134.09	74.41	1.742	33.00	19.91	3.70	17.44	184.90	72.57
1.0E-03		0.540	45.56	37.87	2350.17	35.39	131.12	74.49	1.700	34.62	19.96	3.64	17.48	184.97	72.63
5.0E-03		0.520	47.58	38.01	2397.65	35.53	130.93	74.57	1.680	35.38	20.19	3.87	17.71	184.47	72.71
1.0E-02		0.500	49.60	36.32	1178.79	33.84	136.91	74.66	1.620	37.69	19.69	3.07	17.22	186.39	72.79
0.0		SDS	0.992		24.67	20.33	22.19	170.60	73.05	2.6	21.54	10.40	<b>19.06</b>	176.24	71.61
5.0E-07	0.674		32.06	28.90	79.22	26.42	159.31	73.92	2.182	16.08	21.34	7.55	18.86	178.90	72.20
1.0E-06	0.640		35.48	30.85	166.04	28.38	153.16	74.04	1.880	27.69	15.33	0.68	12.85	198.96	72.17
5.0E-06	0.600		39.52	32.98	373.24	30.49	146.46	<b>74.16</b>	1.840	29.23	16.17	0.92	13.70	196.43	72.26
1.0E-05	0.588		40.73	33.00	365.86	30.52	146.57	74.22	1.800	30.77	16.76	1.13	14.28	194.69	72.33
5.0E-05	0.500		49.60	40.13	5722.98	37.65	123.72	74.54	1.770	31.92	19.74	3.50	17.26	185.31	72.51
1.0E-04	0.475		52.12	40.72	6969.12	38.24	122.11	74.65	1.710	34.23	19.73	3.36	17.25	185.67	72.61
5.0E-04	0.450		54.64	42.18	11875.64	39.70	117.60	74.77	1.650	36.54	18.77	2.23	16.28	189.06	72.66
1.0E-03	0.406		59.07	45.83	48458.10	43.35	106.03	74.96	1.632	37.23	20.11	3.64	17.63	184.96	72.78
5.0E-03	0.360		63.71	49.93	224188.99	47.46	93.23	75.25	1.600	38.46	20.66	4.36	18.18	183.47	72.88
1.0E-02	0.300		69.76	<b>54.30</b>	1101567.49	51.82	79.92	75.65	1.550	40.38	21.36	5.54	18.88	181.50	73.00
0.0	CPC		0.992		24.67	20.33	22.19	170.60	73.05	2.6	21.54	10.40	<b>19.06</b>	176.24	71.61
5.0E-07		0.685	30.95	29.85	118.18	27.37	156.02	73.89	2.520	3.08	21.71	10.11	19.29	176.50	71.91
1.0E-06		0.662	33.27	31.14	190.99	28.66	151.99	73.98	2.500	3.85	22.82	14.91	20.34	173.21	72.00
5.0E-06		0.651	34.38	31.41	208.98	28.94	151.25	74.03	2.460	5.38	26.81	68.18	24.33	160.54	72.20
1.0E-05		0.640	35.48	31.82	242.80	29.35	150.05	74.08	2.430	6.54	29.35	179.87	26.87	152.49	72.34
5.0E-05		0.632	36.29	32.03	257.81	29.55	149.51	74.13	2.400	7.69	29.63	198.78	27.15	151.71	72.38
1.0E-04		0.612	38.31	32.95	362.21	30.47	146.66	74.19	2.370	8.85	29.61	192.91	27.13	151.92	72.42
5.0E-04		0.582	41.33	35.03	806.13	32.55	140.06	74.31	2.320	10.77	29.94	213.21	27.46	151.05	72.49
1.0E-03		0.652	34.27	32.35	296.55	29.87	148.34	74.10	2.360	9.23	28.40	121.78	25.92	155.73	72.35
5.0E-03		0.754	23.99	26.98	31.57	24.50	165.14	73.74	2.400	7.69	26.93	70.96	24.45	160.27	71.24
1.0E-02		0.806	18.75	24.06	13.63	21.59	<b>173.00</b>	73.46	2.450	5.77	24.34	26.63	21.86	168.40	72.07

### 3.4. Adsorption isotherm

The information on the interaction between the SAS molecules and metal surface can be provided by the adsorption isotherms. Two main types of interaction can be describing the adsorption behavior of the organic compound: physical adsorption and chemical adsorption. These are related to the chemical structure of the inhibitor, the type of the electrolyte, the charge, and nature of the metal [2]. The adsorption mechanism of SAS on copper surface was determined by fitting the  $\theta$  values to different adsorption isotherms such as Langmuir and Kinetic-thermodynamic model by the following equation [36, 37] :

$$\text{Langmuir: } C/\theta = 1/K + C \tag{8}$$

$$\text{Kinetic-thermodynamic: } (KC)^y = (\theta / 1 - \theta) \tag{9}$$

where  $\theta$  is the surface coverage  $\theta = \frac{I_{L(blank)} - I_{L(SAS)}}{I_{L(blank)}}$  , K is the adsorption equilibrium constant,

C is the concentration of SAS and y is the number of SAS molecules occupying a given active site.

Though the plot of C/θ versus C was linear (R<sup>2</sup>= 0.999). Although these plots are linear, the gradients are never unity, Contrary to what is expected for the ideal Langmuir adsorption isotherm

equation. The departure in the values of the slopes of Langmuir from unity may be advocated to be due to the mutual interaction between adsorbed molecules in close vicinity. SAS having polar atoms or groups which are adsorbed on the metal surface may interact by mutual repulsion or attraction [38, 39].

Linear- relationship can be obtained on plotting  $\log \theta/1-\theta$  as a function of  $\log C$  for all SAS at 25°C as shown in Fig.8. It is seems from Table 3 that, large values of K means better and strong interaction. It is obvious that, the values of 1/y greater than unity imply the formation of multilayer of the SAS on the copper surface [40]

The adsorptive equilibrium constant (K) is related to the standard adsorption free energy ( $\Delta G^{\circ}_{ads}$ ) obtained according to [41]:

$$\Delta G^{\circ}_{ads} = -RT \text{Ln} (55.5 K) \tag{10}$$

Generally, value of  $\Delta G^{\circ}_{ads}$  up to -20 kJ /mol is consistent with the electrostatic interaction between the charged molecules and the charged metal (physical adsorption) while the value more negative than 40 kJ/ mol involve sharing or transfer of electrons from the inhibitor molecules to the metal surface to form a co-ordinate type of bond (chemisorption) [41]. At all SAS studied, the values  $\Delta G^{\circ}_{ads}$  are less negative than -40 kJ/ mol so,  $\Delta G^{\circ}_{ads}$  values designate that the adsorption mechanism of SAS on copper surface in 8 M H<sub>3</sub>PO<sub>4</sub> using RDE and RCE is physical adsorption. The negative value of  $\Delta G^{\circ}_{ads}$  indicated that the adsorption of SAS molecules was spontaneous process [42, 43].

**Table 3.** linear fitting parameters and calculated values of free energy of adsorption- $\Delta G_{ads}$ (kJ mol<sup>-1</sup>) for different surfactants at 25°C for RCE and RDE at 375 rpm.

Electrode	RCE				RDE					
Kinetic-thermodynamic adsorption isotherm										
Surfactant	y	1/y	K	R <sup>2</sup>	$-\Delta G^{\circ}_{ads}$ (kJ/mol)	y	1/y	R <sup>2</sup>	K	$-\Delta G^{\circ}_{ads}$ (kJ/mol)
Triton x-100	0.16	5.93	$7.51 \times 10^3$	0.99	32.06	0.064	15.62	0.98	$2.04 \times 10^3$	28.83
SDS	0.12	8.22	44.05	0.98	19.33	0.149	6.70	0.98	$1.90 \times 10^3$	28.65
CPC	0.21	4.59	26.48	0.98	18.06	0.057	17.28	0.98	2.84	12.54

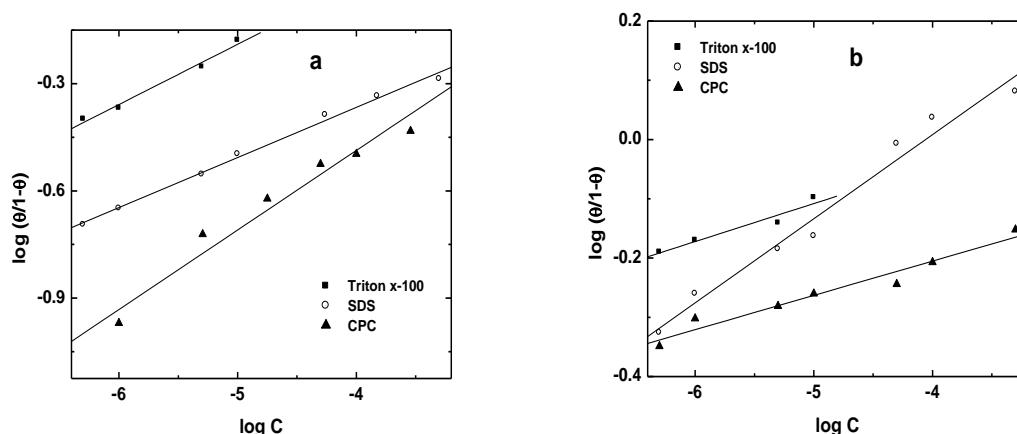


**Figure 8.** Kinetic-thermodynamic adsorption isotherm at 375 rpm and 25°C in the presence of SAS using a) RCE and b) RDE.

### 3.5. Data correlation

Dimensionless analysis using mass transfer concepts showed that the dissolution when controlled by diffusion of one of the species between the bulk fluid and the surface could be modeled completely by the rate of mass transfer on the rate limiting species.

When the fluid flow is generated entirely by RCE and RDE, the characteristic of mass transport conditions can be described by a dimensionless group correlation of the following form:

$$Sh = a Re^b Sc^{0.33} \quad (11)$$

where the Sherwood number ( $Sh = kd/D$ ) describes mass transport by forced convection, the Reynolds number ( $Re = Ud/\nu$ ) is an indication of the fluid flow regime, and the Schmidt number ( $Sc = \nu/D$ ) relates the electrolyte transport properties. The average mass transport coefficient is  $k$ ,  $\text{cm sec}^{-1}$  ( $k = i_L/zFC_{Cu^{2+}}$ ),  $d$  is the diameter of the rotating electrode (cm),  $D$  is the diffusion coefficient ( $\text{cm}^2.\text{sec}^{-1}$ ),  $U$  is the peripheral velocity ( $U = \omega r$ ,  $\text{cm sec}^{-1}$ ),  $\nu$  is the kinematic viscosity ( $\text{cm}^2.\text{sec}^{-1}$ ) and  $a$ ,  $b$  are constants [44].

By plotting  $\log Sh/Sc^{0.33}$  and  $\log Re$  a straight line was obtained; its slope gives constant  $b$  and intercept give the constant  $a$ . Fig.9 shows the mass transfer correlation for all parameters used in case of RCE and RDE. From this figure, the data can be correlated by the following equations:

$$Sh = 0.165 Sc^{0.33} Re^{0.69} \pm 0.0092 \quad \text{for RCE}$$

$$Sh = 0.912 Sc^{0.33} Re^{0.499} \pm 0.0011 \quad \text{for RDE}$$

The exponent in equation for RCE denotes a highly turbulent flow [44], which agree with the previous mass transfer study in aqueous media while the exponent in the equation for RDE denotes laminar flow which agrees with the previous mass transfer studies in aqueous media [9], also the high value of Schmidt number in case of RDE indicates that the diffusion layer lie well within the laminar sub layer [7].

### 3.6. Effect of alcohols

To study the effect of addition of alcohols (1-5 ml) on the dissolution rate of copper in 8M  $H_3PO_4$ , four different types of alcohols were used (methanol, ethanol, propanol and butanol). Fig 10 shows the effect of alcohols volumes on the copper dissolution at 25°C and 500 rpm. Addition of alcohols was found to decrease the limiting current of dissolution process (Table 4) and this behavior may be attributed to the following:

1- The low dielectric constant of alcohols leads to a decrease of the activity of copper ions to ion pair formation with a consequent decrease in the dissolution rate.

2- The addition of alcohols decrease the diffusivity of ions in the solution by changing the composition of solvation shell [45].

The percentage reduction in dissolution process was found to decrease in the order: butanol > propanol > ethanol > methanol. This may be explained as the hydrophobic character increase as the length of hydrocarbon chain in alcohols increases so the molecules becomes more hindered to mass transfer processes.

Addition of alcohols to 8M H<sub>3</sub>PO<sub>4</sub> containing 1 × 10<sup>-4</sup>M SAS, lead to decrease in limiting current of dissolution process and increase in inhibition efficiency percentage. This inhibition efficiency depends on the type of alcohols and SAS and their concentration .These result indicate that the efficiency of the surfactant is increased by alcohols addition which acts as co-surfactants [46].

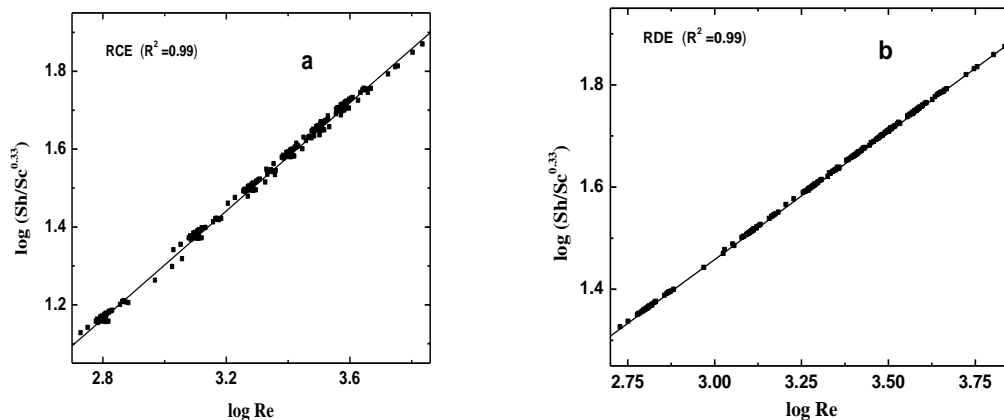


**Figure 9.** The overall mass transfer correlation for dissolution process in the absence and presence of different SAS at 25°C for a) RCE and b) RDE.

**Table 4.** The effect of mixed surfactants –alcohols on the limiting current for 8 M H<sub>3</sub>PO<sub>4</sub> at 25°C,500 rpm , RCE

Alcohols volume	Alcohols	IE %	1×10 <sup>-4</sup> mol/l SAS	IE %	Triton x-100+ alcohols	SDS + alcohols	CPC + alcohols	
1ml	Methanol	6.93	Tritonx-100	27.42	28.21	28.96	<b>26.73</b>	
2 ml		7.92			28.61	29.60	<b>27.42</b>	
3 ml		8.81	SDS		29.45	30.69	<b>28.22</b>	
4 ml		9.90			30.11	31.38	<b>28.96</b>	
5 ml		10.89			30.99	32.08	<b>29.70</b>	
1ml	Ethanol	7.82	Tritonx-100	27.42	28.91	29.60	<b>27.23</b>	
2 ml		8.81			29.60	30.69	<b>27.97</b>	
3 ml		9.41	SDS		28.22	30.69	31.13	<b>28.71</b>
4 ml		10.30			31.33	31.68	<b>29.70</b>	
5 ml		11.24			31.93	32.67	<b>30.69</b>	
1ml	Propanol	8.81	Tritonx-100	27.42	29.45	30.20	<b>28.22</b>	
2 ml		9.41			30.10	31.28	<b>29.10</b>	
3 ml		10.15	SDS		28.22	31.29	32.17	<b>29.70</b>
4 ml		10.89			31.68	32.67	<b>30.69</b>	
5 ml		11.88			32.38	33.66	<b>31.58</b>	
1ml	Butanol	9.8	Tritonx-100	27.42	30.69	30.69	<b>29.20</b>	
2 ml		10.89			31.69	31.72	<b>30.24</b>	
3 ml		11.78	SDS		28.22	32.27	32.18	<b>31.18</b>
4 ml		12.77			32.92	33.17	<b>32.18</b>	
5 ml		13.66			CPC	14.75	<b>34.40</b>	34.55

Alcohol can be solubilized among the polar groups of surfactant molecules in the ad-micelle formed at the liquid–solid interface. The existence of alcohol in the ad-micelle will enlarge the space among the polar groups of surfactant molecules and decrease the contact of copper surface with the acid solution. Therefore, the inhibition efficiency can be increased and the dissolution rate can be

decreased by the addition of alcohol. It is observed that, there is a synergism between SAS and alcohols (co-surfactants). Synergism parameter ( $S_\theta$ ) can be calculated using the following equation [47, 48]

$$S_\theta = 1 - \theta_{1+2} / (1 - \theta'_{1+2}) \quad (12)$$

Where  $\theta_{1+2} = (\theta_1 + \theta_2) - (\theta_1 \theta_2)$ ,  $\theta_1$  and  $\theta_2$  are the degree of surface coverage in presence of surfactant and alcohols respectively and  $\theta'_{1+2}$  is the degree of surface coverage in presence of both species. It is noticed that all values of  $S_\theta$  were approximately unity. This may suggest that the inhibition efficiency enhanced by the addition of alcohols to surfactant in 8M  $H_3PO_4$  and a synergistic effect is obtained as a result as a co-operative adsorption between SAS and alcohols [49, 50].

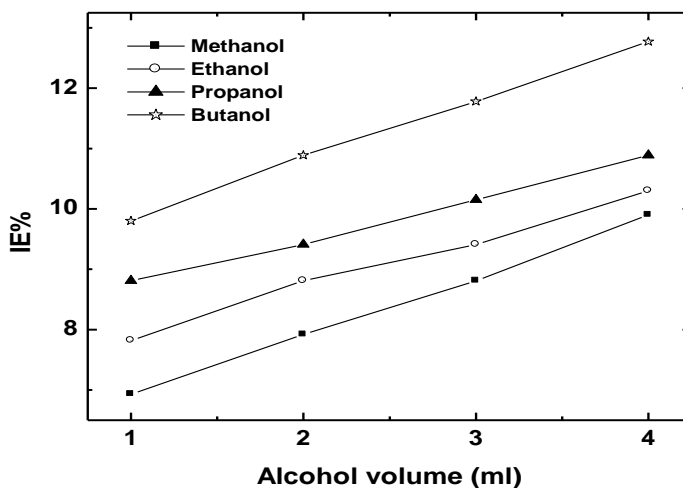


**Figure 10.** Effect of alcohols type on inhibition efficiency percentage (IE %) of dissolution process for copper RCE at 500 rpm and 25 °C.

### 3.7. Scanning electron microscope (SEM)

Fig.11 shows the SEM image for copper surface before dissolution in which a rough, matt and uneven surface was seen also large deep cavities and small pits are distributed over the surface. Fig (12a-c) shows the surface morphology of copper RDE that were dissolved at 25°C with different rotations speeds 250,500 and 750 rpm in 8 M  $H_3PO_4$ . A bad and uneven surface appearance is obtained specially at higher rotation speed, 750 rpm (Fig 12.c) where cavities and large deep pits are represented. We can say that, the radial flow for diffusion of the  $Cu^{2+}$  is disturbed at higher rotation speed which leads to dissimilar dissolution of copper RDE. According to the dreadful appearance of copper RDE at 750 rpm, we used a constant rotation speed of 750 rpm to study the dissolution behavior of copper RDE in presence of SAS,  $1 \times 10^{-2}$  M Triton x-100,  $1 \times 10^{-2}$  M SDS and  $5 \times 10^{-4}$  M CPC (Fig.12d-f). The surface appearance is enhanced in presence of SAS in which smooth and completely uniform surface is obtained. This behavior is attributed to the involvement of SAS molecules in the reaction sites of copper surface and this result indicates that the SAS molecules hinder the dissolution of copper by formation of protective film on copper surface.

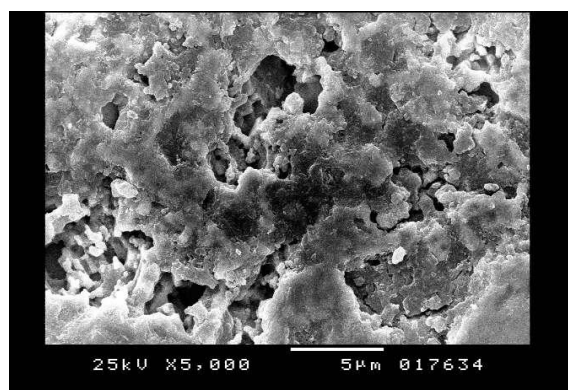


**Figure 11.** Raw sample (before EP)

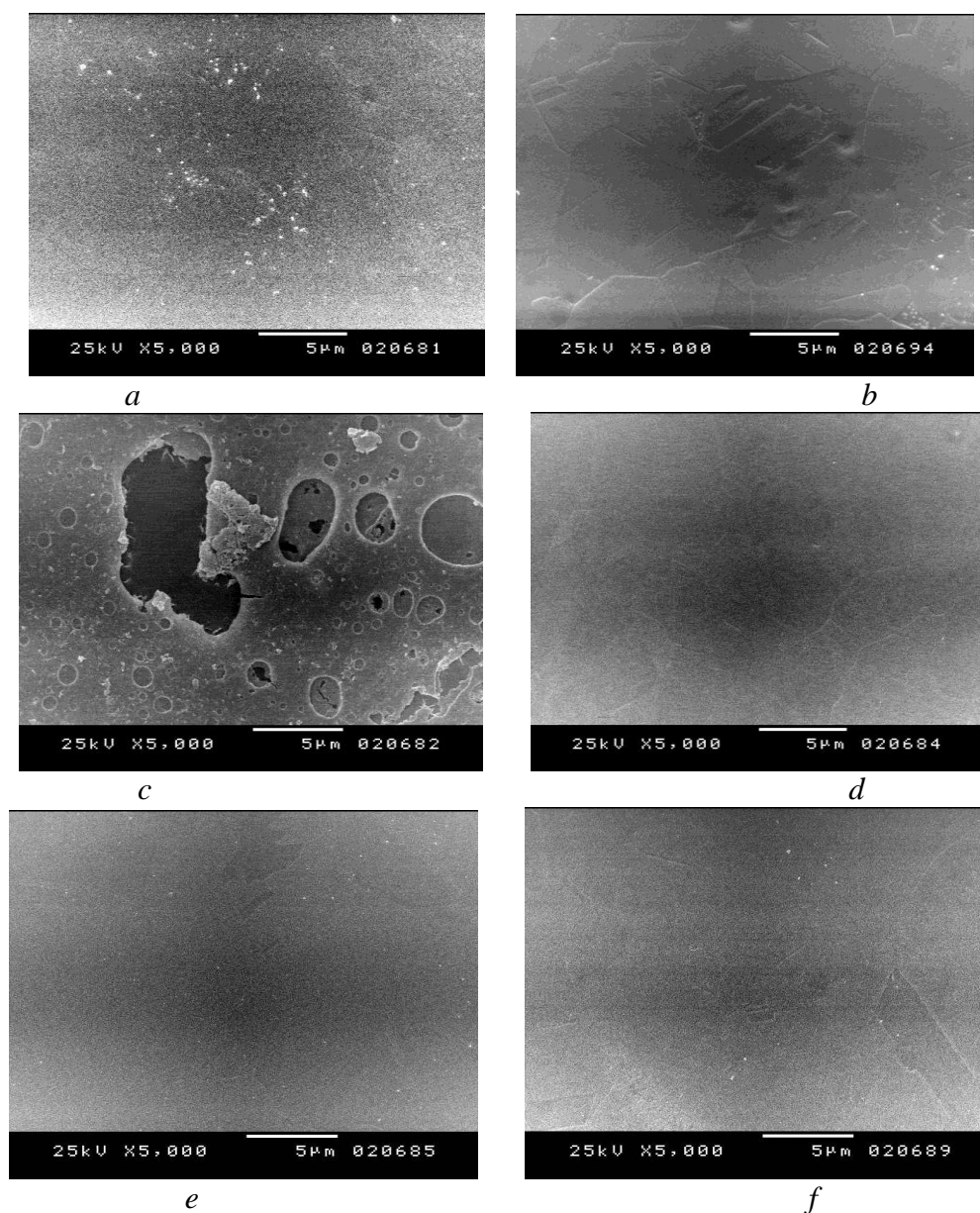


**Figure 12.** surface morphologies of the copper RDE at 25°C after electrodisolution in 8M H<sub>3</sub>PO<sub>4</sub> a) 250 rpm , b) 500 rpm , c) 750 rpm , d) 750 rpm in presence of 1× 10<sup>-2</sup> M Triton x-100 , e) 750 rpm in presence of 1× 10<sup>-2</sup> M SDS and f) 750 rpm in presence of 1× 10<sup>-2</sup> M CPC.

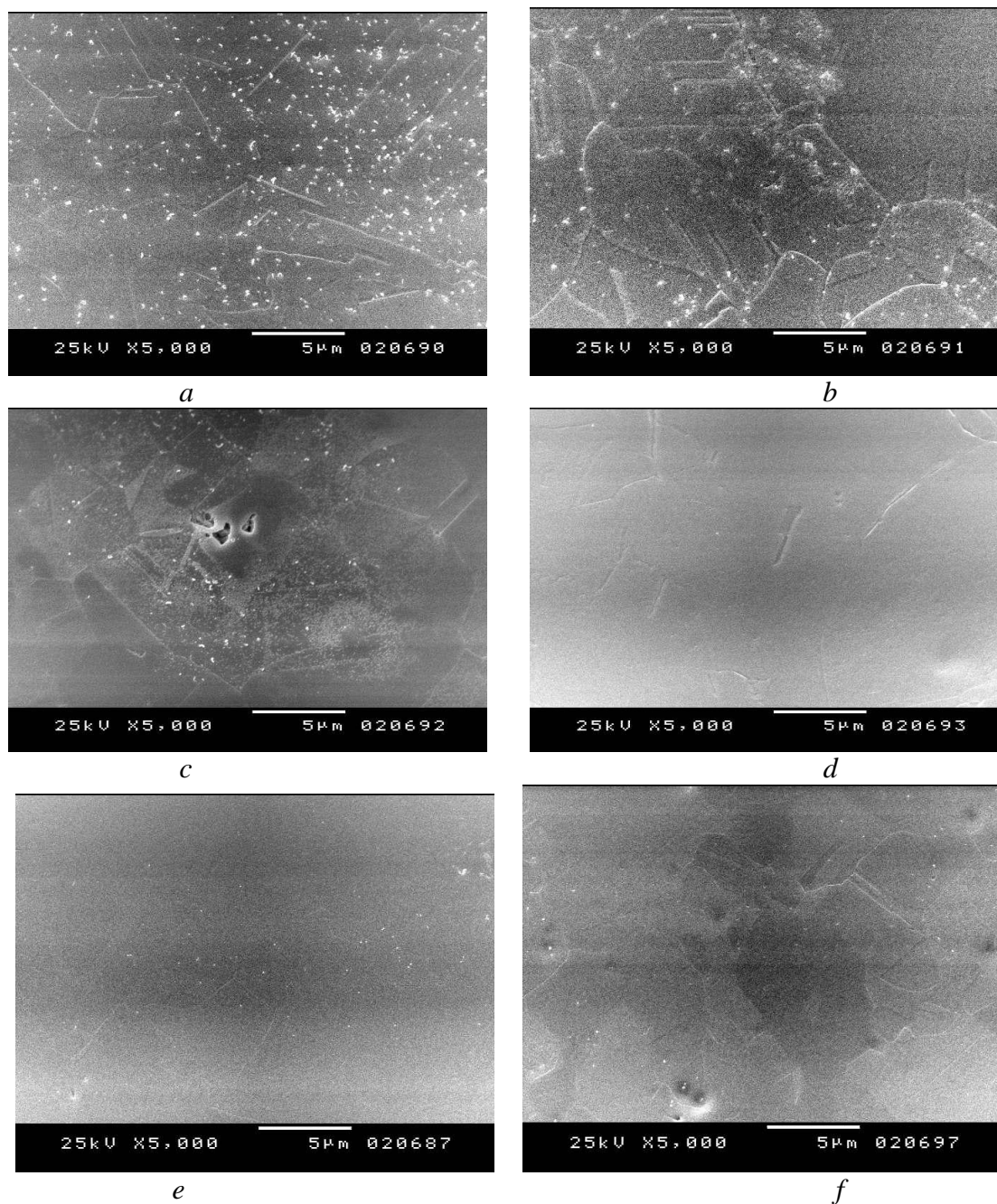


**Figure 13.** surface morphologies of the copper RCE at 25°C after electrodisolution in 8M  $\text{H}_3\text{PO}_4$  a) 250 rpm , b) 500 rpm , c) 750 rpm , d) 750 rpm in presence of  $1 \times 10^{-2}$  M Triton x-100 , e) 750 rpm in presence of  $1 \times 10^{-2}$  M SDS and f) 750 rpm in presence of  $1 \times 10^{-2}$  M CPC.

Fig .13a-c shows SEM – micrograph of the surface morphologies of the copper RCE were dissolved in 8 M  $\text{H}_3\text{PO}_4$  at 25°C with different rotations speeds 250, 500 and 750 rpm. Only a slight difference in the surface morphology was observed in which grain boundaries and small pits are represented clearly at 750 rpm (Fig.13c). We can conclude that, the axial flow as result of RCE for diffusion of the  $\text{Cu}^{2+}$  is significantly affected on the surface quality obtained specially at higher rotation speed. So we will study the dissolution behavior of copper RCE in presence of SAS at 750

rpm (Fig.13d-f), the copper specimen has a better morphology and uniform surface compared with the absence of SAS which reflects the higher adsorption ability of SAS molecules, leading to filling up of grain boundaries which leads to higher inhibition efficiency of the three studied SAS.

#### 4. CONCLUSIONS

- As the rotation rate of the electrodes (RDE &RCE) increases the measured value of limiting current of dissolution process also increase.
- With increasing the concentration of the used SAS, the limiting current decreases and their inhibition efficiency due to their tendency towards adsorption.
- $E_a$  values of SAS were found to be larger than that of  $8\text{MH}_3\text{PO}_4$  free solution, suggesting that the adsorption of SAS molecules leads to an increase in energy barrier of copper dissolution.
- The adsorption of SAS obeys Kinetic –thermodynamic isotherm which indicates that the main process of inhibition is adsorption and values of  $\Delta G^{\circ}_{\text{ads}}$  indicate that the adsorption process is physical adsorption.
- In presence of the three studied surfactant, surface morphology enhanced for RDE and RCE copper surface at high rotation speed.
- The values of synergism parameter ( $S_0$ ) are approximately unity showing the dissolution inhibition brought about by SAS with alcohols is synergistic in nature and co-operative adsorption between SAS and alcohols prevails over competitive adsorption.

#### References

1. S. S. Mahmoud , *Corros. Prot. Mater.*,26 (2)(2007) 53.
2. D.Özkır, K.Kayakırılmaz, E. Bayol, A.A Gürten, F.Kandemirli, *Corros. Sci.* , 56(2012) 143.
3. X. Li, G.Zhang, J. Dong, X.Zhou, X.Yan, M. Luo, *Theochem.*,710 (2004) 119.
4. R. Fuchs-Godec, *Electrochim. Acta.*, 54 (2009) 2171.
5. A.R.Katritzky,L.M.Pacureanu,S.H.Slavov, D.A.Dobchev, D.O.Shah , M.Karelson, *Comput. Chem. Eng.*, 33(2009)321.
6. R. G.-Martínez, J.M-Flores, R. D-Romero, and J. G-Llongueras, *Afinidad* .,62 (519) (2005) 448.
7. M.Bilson and K.Bremhorst , Comparison Of Turbulent Scalar Transport in A Pipe and A Rotating Cylinder . Third International Conference on CFD in The Minerals and Process Industries. CSIRO, Melbourne , Australia . 10-12 December 2003 .
8. X. Li ,S.Deng , H.Fu, *Corros. Sci.* ,53 (2011) 664.
9. A.A.Taha , *Anti-Corros. Method Mater.*, 47(2)(2000)94.
10. S. M Abd El-Haleem, A.M.Ahmed and A.E.El- Nagger, *J. Dispersion Sci. Technol.*, 31(4)(2010)512.
11. N. M. Elmalah, S.M.Abd Elhaliem, A.M.Ahmed and, S .M.Ghozy, *Int. J. Electrochem. Sci.*,7 (2012) 7720.
12. H.H. Abdel Rahman, A.H.E. Moustafa1, M.K. Awad, *Int. J. Electrochem. Sci.*, 7 (2012) 1266 .
13. A.A.Taha , H.H. Abdel Rahman , F.M.Abouzeid. *Int. J. Electrochem. Sci.*,8(2013) 6744.
14. M. Eisenberg, C.W. Tobias and C.R. Wilke, *J. Electrochem. Soc.*, 101 (1954) , 306.

15. X.Li,S.Deng ,G.Mu, H.Fu, F.Yang, *Corros.Sci.*50(2008)420.
16. N.A.Negm,N.G.Kandile, E.A.Badr, M.A .Mohammed.*Corros.Sci.*65(2012)94.
17. M.A. Hegazy, A.S. El-Tabei, H.M. Ahmed, *Corros. Sci.*, 64(2012)115.
18. M.P. Desimone , G. Gordillo , S.N. Simison. *Corros. Sci.*, 53 (2011) 4033.
19. I. Esih, T. Soric, Z. Pavlinic, *Corros. J.* ,33 (1998) 309.
20. V. Jovancicevic, S. Ramachandran, P. Prince, *Corrosion* ,55(1999) 449.
21. S.A.Abd El-Maksoud, *J. Electroanal. Chem.*, 565 (2004) 321.
22. D.A.Szanto,S.Cleghorn, C.P.De-Leon , F.C.Walsh. *AIChE.*,54(3)(2008)802.
23. R.D.Grimm and D.Landolt , *Corros. Sci.* ,36 (1994) 1847.
24. J.F. Aebersold , P.A. Stadelmann and M. Matlosz, *Ultramicroscopy* ,62 ( 1996) 157.
25. K. Fushimi,, H. Kondo and H. Konno. *Electrochim. Acta* .,55 (2009) 258.
26. 26. O. Piotrowski, C. Madore and D. Landolt , *Electrochim. Acta.*,44 (1999) 3389.
27. L. Neelakantan, A. Pareeka, A. W. Hassel ,*Electrochim. Acta* .56 (2011) 6678.
28. L.Li,Q.Qu,W.Bai,F.Yang,Y.Chen,S.Zhang,Z.Ding,*Corros.Sci.*59(2012)249.
29. M.M.Solomon,U.A.Umoren,I.I.Udosoro,A.P.Udoh,*Corros.Sci.*52(2010)1317.
30. R. Fuchs-Godec.*Colloid.Surf.A.*280(2006)130.
31. L.G-Qin, Y.Wu,Y.M-Wang, X.Jiang, *Corros.Sci.*50(2008)576.
32. G. Mu, X. Li, G. Liu, *Corros. Sci.*, 47 (2005) 1932.
33. S. S. Al-Juaid, *Portug. Electrochim. Acta* .,25 (2007) 363.
34. Z. Tao, S. Zhang, W. Li, B. Hou, *Corros. Sci.* ,51 (2009) 2588.
35. I. Langmuir, *J. Am. Chem. Soc.* 40 (1918) 1361 .
36. A.A. El-Awady, B.A. Abd-El-Nabey, S.G. Aziz, *J. Electrochem. Soc.* 139 (1992) 2149.
37. M. Yadav ,U. Sharma, *J. Mater. Environ. Sci.*, 2 (4) (2011) 407.
38. J. Hmimou , A. Rochdi , R. Touri , M. Ebn Touhami , E. H. Rifi , A. El Hallaoui , A. Anouar , D. Chebab, *J. Mater. Environ. Sci.*, 3 (3) (2012) 543.
39. J.M. Bastidas . P. Pinilla , E. Cano, J.L. Polo and S. Miguel . *Corros. Sci.*, 45 (2003) 427.
40. E. Cano, J.L. Polo, A. La Iglesia, J.M. Bastidas, *Adsorption.* ,10 (2004) 219.
41. S. Zhang , , Z. Tao, S. Liao and F.Wu ,*Corros. Sci.* ,52( 9)( 2010) 3126.
42. A. Yurt, S. Ulutas and H. Dal, *Appl. Surf. Sci.*, 253 (2006) 919.
43. A. Recéndiz, S. León, J. L. Nava, F. F. Rivera. *Electrochim. Acta.*, 56 (2011) 1455.
44. H.H. Abdel Rahman, A.H.E. Moustafa' , S.M.K. Abdel Magid, *Int. J. Electrochem. Sci.* 7(2012) 6959.
45. M.H.Abdel-Aziz. *Hydrometallurgy*, 109 (2011)161.
46. A.Meziani, D.Touraud, A.Zradba, M.Claysse, W.Kunz, *J. Molec., Liq.*84 (2000)301.
47. E.E. Ebenso, *Mater. Chem. Phys.* ,79 (2003) 58.
48. M.A. Migahed, M.A. Hegazy, A.M. Al-Sabagh, *Corros. Sci.*, 61 (2012) 10.
49. G.Y. Elewady,I.A.El-Said , A.S.Fouda, *Int. J. Electrochem. Sci.*, 3 (2008) 177.
50. A.Khamis,M.M.Saleh,M.H.Awad, *Corros.Sci.*66(2013)343